METEOSAT DERIVED PLANETARY TEMPERATURE TREND 1982-2006

by

Andries Rosema, Steven Foppes, Joost van der Woerd
(The Netherlands)

Reprinted from

ENERGY &
ENVIRONMENT

VOLUME 24 No. 3 & 4 2013

MULTI-SCIENCE PUBLISHING CO. LTD.
5 Wates Way, Brentwood, Essex CM15 9TB, United Kingdom

METEOSAT DERIVED PLANETARY TEMPERATURE TREND 1982-2006

Andries Rosema, Steven Foppes, Joost van der Woerd
EARS Earth Environment Monitoring Ltd, Delft, the Netherlands
Kanaalweg 1, 2628 EB Delft, the Netherlands, Email: info@ears.nl

ABSTRACT
24 year of Meteosat hourly thermal infrared data have been used to study planetary surface temperature change. Thermal infrared radiation in the 10.5-12.5mm spectral window is not affected by CO2 and only slightly by atmospheric water vapor. Satellite thermal infrared data have been converted to brightness temperatures as prescribed by Eumetsat. Hourly brightness temperature images were then composed to corresponding noon and midnight temperature data fields. The resulting data fields were cloud filtered using 10, 20 and 30 day maximum temperature substitution. Filtered data were subsequently averaged for two 10 yearly periods: 1986-1995 and 1996-2005. Finally the change in brightness temperature was determined by subtraction. In addition nine locations were selected and data series were extracted and studied for the period 1982-2006. Our observations point to a decrease in planetary temperature over almost the entire hemisphere, most likely due to an increase of cloudiness. Two small areas are found where a considerable temperature increase has occurred. They are explained in terms of major human interventions in the hydrological balance at the earth surface.

1. INTRODUCTION

EARS Earth Environment Monitoring is providing Meteosat based water and climate services. To this end, Meteosat visual and thermal infrared images are received hourly and processed to hemispheric data fields of surface and boundary layer temperature, global and net radiation, actual and potential evapotranspiration, as well as precipitation. These data are then applied in drought monitoring, crop yield forecasting [1,2] and river flow forecasting systems. Since 2009, EARS is also developing drought and excessive precipitation insurance [3]. For this purpose a 30 year data base of hourly Meteosat visual (VIS) and thermal infrared (TIR) images has been composed. In this study we have used these data to study recent change in planetary temperature.

The subject is topical as during the past decades the fear has developed that by the burning of fossil fuels and the resulting increase in atmospheric CO2 content, mankind is seriously affecting climate beyond its natural variability and to an extent that will

appear to be detrimental to plant, animal and human live. This fear has been driven by time series of temperature measurements at meteorological stations, which show an overall temperature increase of 0.074 K/decade during the last 100 year, increasing to 0.177 K/decade when considering the last 30 year [4]. These air temperature measurements are taken at 1.5-2 meter height, in an environment that during the past century has progressively undergone changes in surface conditions due to urbanization, road building and drainage. In the Netherlands, for example 10 percent of the national area currently consists of hardened surface. Such changes may have a significant effect on local air temperatures. Therefore there is a need to supplement these near surface local air temperature observations with large scale temperature observations from satellites.

The first analysis of satellite data in relation to this subject was conducted at the University of Alabama [4,5], later followed by the company Remote Sensing Systems [6]. Use was made of microwave sounding units (MSUs) on board of polar orbiting NOAA satellites since 1979. These instruments measure the oxygen microwave emission in a number of dedicated frequency channels. These measurements represent a weighted temperature average of a thick layer of atmosphere. MSU channel 4 represents the temperature of the lower stratosphere with a main point at 17 km height. MSU channel 2 spans the troposphere, having its effective height at 3-4 km. An additional so-called lower troposphere synthetic product derived from this channel (using variations in swath angle) has an effective height of 0.8 km.

The early work at the University of Alabama showed a slight cooling of the troposphere during the 1980's. This result was later criticized. A range of corrections was considered necessary. The final outcome and current state of the art as presented in the IPCC 4th Assessment Report is (a) a cooling of lower stratosphere by about 0.4 K/decade and (b) a temperature increase of about 0.1 K/decade in the troposphere [7].

We are not aware of attempts to study the global warming issue by measuring the earth surface ("skin") temperature from satellite, making use of thermal infrared bands in which the atmosphere is largely transparent. In this study, we use the 10.5-12.5 mm infrared wavelength band on board of the Meteosat First Generation (MFG) satellites series. The cloud free atmosphere is largely transparent for thermal radiation in this range. There is no effect of ozone and only a minor effect of water vapor. As global warming is expected to occur both at the earth surface and in the lower atmosphere a small interference of atmospheric water vapor will not obscure a possible global warming signal. Clouds, however, are black bodies. They may be recognized and filtered out on the basis of their low cloud top temperature.

The Meteosat satellite series is operated by the European Organization for the Exploitation of Meteorological Satellites (EUMETSAT). Eumetsat is an intergovernmental organization and has 26 member states. The Council is the supreme body of the organization and is composed of representatives from the national meteorological services of the member states. The Meteosat First Generation series has been in orbit from 1977 until 2007 and consisted of 7 satellites: Meteosat 1-7. The present study pertains to the period 1982-2007 covered by Meteosat 2-7.

2. DATA SOURCE AND CALIBRATION

Meteosat is positioned over the equator at zero degree longitude at a distance of about 36000 km. Its orbital angular velocity is equal to the rotation angular velocity of the earth. Therefore the satellite is "geostationary" and remains in the same position relative to the earth surface. This allows for a high observation repeat coverage of the entire hemisphere. In this study, the basic data set consists of hourly thermal infrared images.

The thermal infrared images are coded as raw binary digital numbers or "counts". These have to be converted to brightness temperatures. The calibration procedures are explained in detail on the Eumetsat website [8] and are only briefly addressed here. The first step in to calculate the thermal infrared radiance in the 10.5-12.5 mm infrared window (R) from the satellite counts (C):

$$R = \alpha * (C-C_0) \tag{1}$$

where α is the calibration coefficient, C the digital Meteosat count and C_0 the space count. The latter is the count measured when the scanning system observes space. The calibration coefficient was at least updated twice a day. The radiance (R) may be converted to the equivalent brightness temperature (T). The precise relation depends on the spectral properties of the infrared detection ensemble and is available for each satellite of the MFG series. The applicable calibration coefficients (α) and the radiance to temperature conversion tables are all available from the Eumetsat website [8]. For practical reasons, we approach the radiance to temperature relationship with a natural logarithmic function

$$T = \beta / \{\ln(R) - \gamma\} \tag{2}$$

3. GENERATION OF NOON AND MIDNIGHT TEMPERATURE COMPOSITES

The daily planetary temperature is approximated as the average of noon and midnight temperature. However, when an image is taken at noon on the Greenwhich meridian, i.e. Meteosat position, then it is later to the east and earlier to the west. The image can be considered to be composed of 12 segments, each representing one hour. Consider the 12 hr segment of a Meteosat image taken at noon. Identify a pixel within this segment, but westward of the Greenwhich meridian, where it is x minutes before noon, having a temperature T_{12}. Next, consider an image taken one hour later, i.e at 13 hrs. The time at the same pixel is 60-x minutes after noon and the temperature measured is T_{13}. The noon temperature (T_n) of this pixel is now obtained by weighed linear interpolation:

$$Tn = [(60-x)*T_{12} + x*T_{13}]/60 \tag{3}$$

With this interpolation approach, the noon temperatures are determined for the entire hemisphere, using the applicable imagery and segments. The result of this data

composition and interpolation procedure is a Meteosat composite image of the hemisphere that shows in every pixel the noon planetary temperature. In the same way, a composite is generated that represents the midnight planetary temperature.

4. DATA SET

Our total data set consists of hourly Meteosat First Generation (MFG) data for the period 1982-2006 and Meteosat Second Generation (MSG) data for the period 2005-date. We have processed all data to daily noon and midnight brightness temperature composites. By averaging the noon and midnight temperature composites an hemispheric data field of the daily average planetary temperature is obtained.

The MSG data have a higher spatial resolution (3 km sub satellite) than the MFG data (5 km sub satellite). For this study we have only used MFG data corresponding to the period 1982-2005.

5. FILTERING CLOUDS

The noon and midnight temperature composite images contain the effects of clouds. We have removed these by applying a numerical filtering technique. Clouds have a considerably lower temperature than the earth surface and will tend to decrease the observed planetary temperature. Every day a surrounding window of e.g. 10 days is considered and the current pixel temperature is replaced by the highest brightness temperature observed in this window. Using this technique, additional data sets were created applying 10, 20 and 30 day maximum temperature filters.

6. DETERMINING TEMPERATURE TRENDS

We want to determine earth surface brightness temperature change all over the hemisphere. To this end, we have processed the noon and midnight temperature composite images in accordance with the following steps:

a) Average noon and midnight temperature composites for the period 1996-2005.
b) Average noon and midnight temperature composites for the period 1986-1995.
c) Subtract averages to obtain noon and midnight temperature trend

This procedure was repeated for the 10, 20 and 30 day filtered data sets. The average temperature trends for the unfiltered and filtered data are shown in figure 1a-d. The various cloud filters have a clear effect. In figure 1a, the unfiltered data, cloud structures are still present. The 10 day filter removes most of the cloud influence (figure 1b). When applying longer filters (figures 1c and 1d) the results converge. The difference between the 20 and 30 day filtered trend is less than 0.1 K/decade for the entire hemisphere.

Figure 2 presents the noon, midnight and average temperature trend images for the 30 day filtered data. The spatial variations in the midnight temperature trend are relatively small. The variation in the noon and average temperature trend is notably larger. Although the temperature trend is almost everywhere negative, the noon and average trend shows some locations with an increase in temperature. For two locations, one in Iraq and one in Tanzania, details are shown in figures 3a-b.

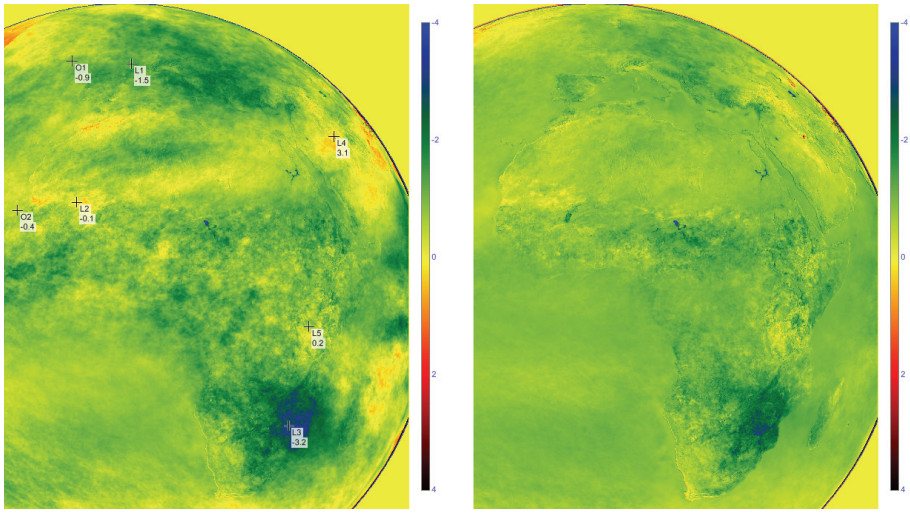

(a) no filter *(b) 10 day filter*

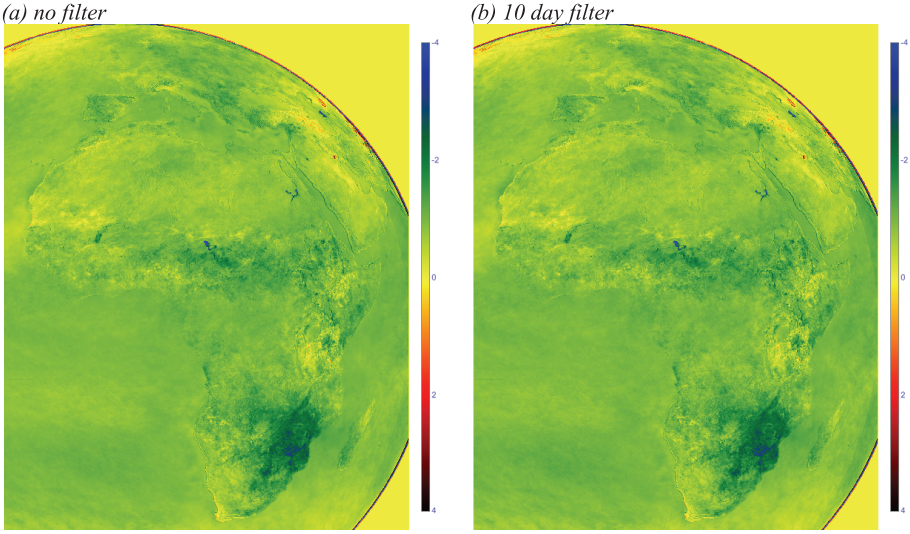

(c) 20 day filter *(d) 30 day filter*

Figure 1a-d: Average planetary brightness temperature trend 1986-2005 for various degree of cloud filtering: (a) unfiltered, (b) 10 day, (c) 20 day and (d) 30 day maximum temperature filter. Scale from -4 (blue) to +4 K/decade (black). Difference between (c) and (d) is less than 0.1 K for the entire hemisphere

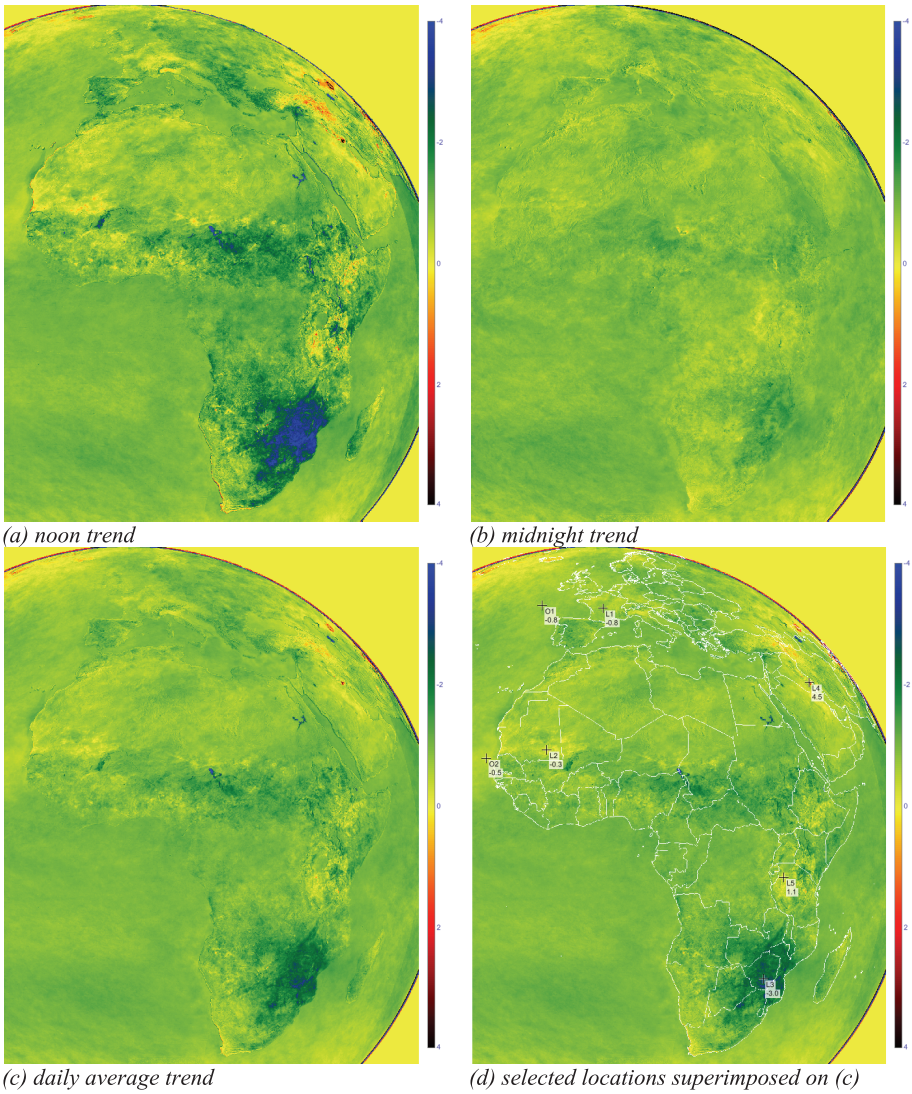

(a) noon trend *(b) midnight trend*

(c) daily average trend *(d) selected locations superimposed on (c)*

Figure 2a-d: Planetary brightness temperature trend during 1986-2005 at noon (a), at midnight (b) and averaged (c). Figure 2d shows the national boundaries superimposed on the average temperature trend (c) and the locations for which temperature time series have been extracted from the data (figure 4-11).

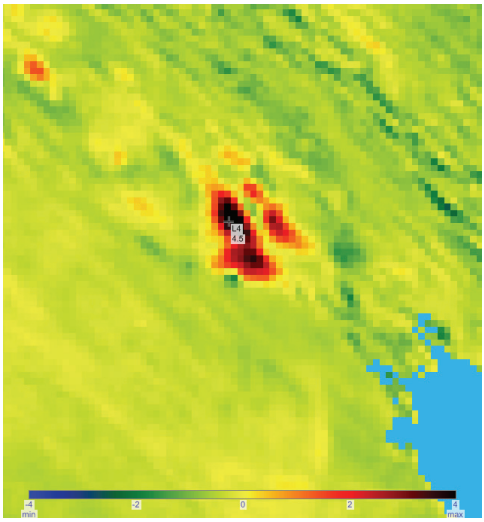

Figure 3a: Location L4 in SE Iraq, showing a +4.5 K per decade average temperature trend due to draining of marshes at the confluence of the Euphrat and Tiger during the years 1993-1995

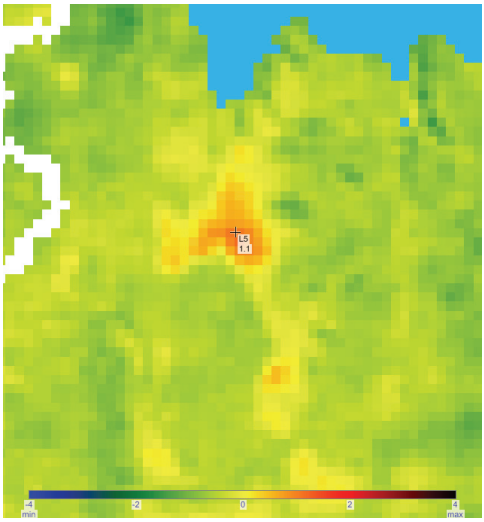

Figure 3b: Location L5 in NW Tanzania south of Lake Victoria, showing +1.1 K per decade average temperature trend, associated with the expansion of mining activities in this area.

7. EXTRACTING TEMPERATURE TIME SERIES

For better insight in the cloud filtering process, we have extracted the daily average temperature time series for location L1, situated in the centre of France for the entire period 1982-2006. These series are shown in figures 4a-d for the non-filtered and 10, 20 and 30 day filtered data respectively. Also the trend lines are shown. From these figures, it is evident that the 10 day filter removes already most of the cloud influence. The longer cloud filters have only a minor effect on the temperature trend.

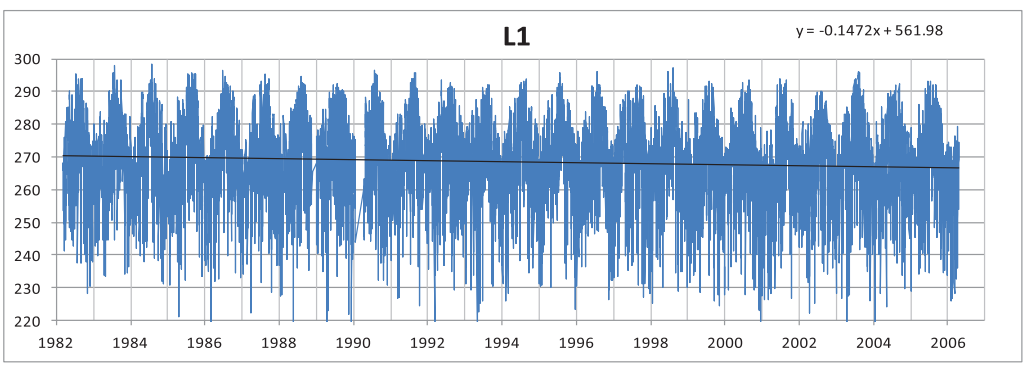

Figure 4a: Unfiltered average planetary temperature time series at location L1 (France)

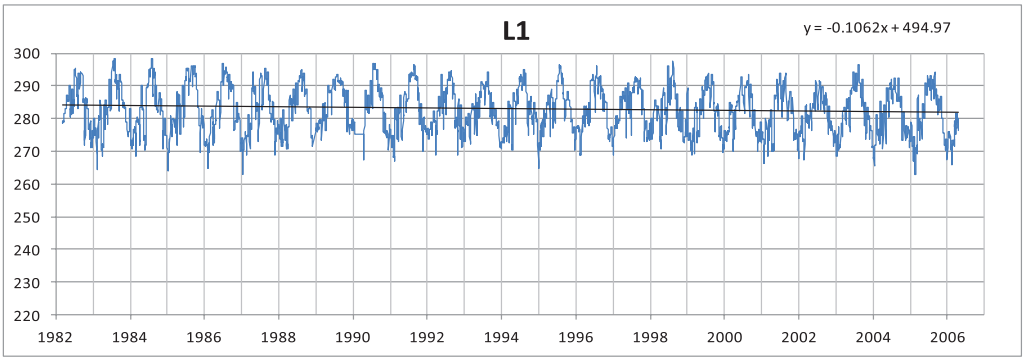

Figure 4b: Idem, 10 day maximum temperature filter applied

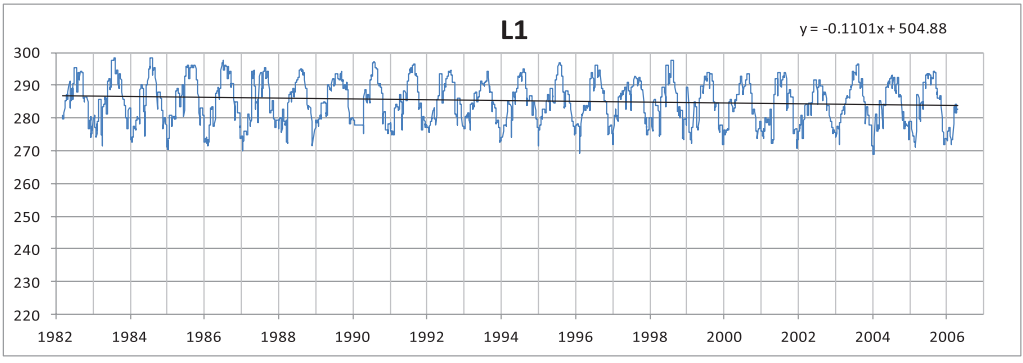

Figure 4c: Idem, 20 day maximum temperature filter applied

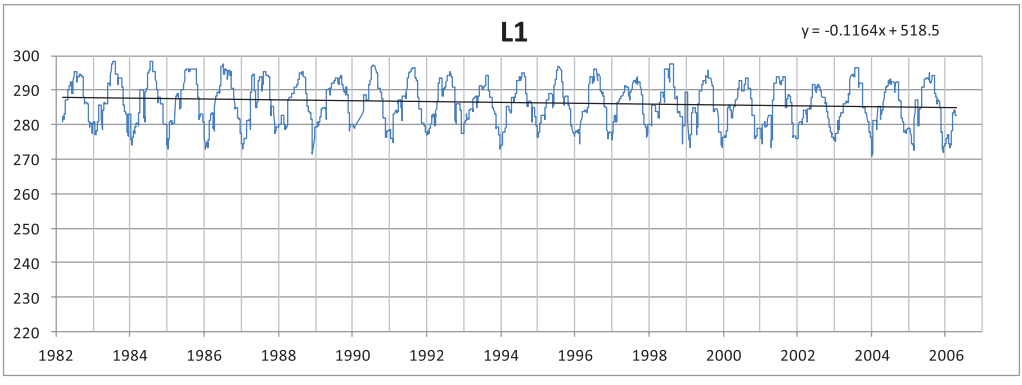

Figure 4d: Idem, 30 day maximum temperature filter applied

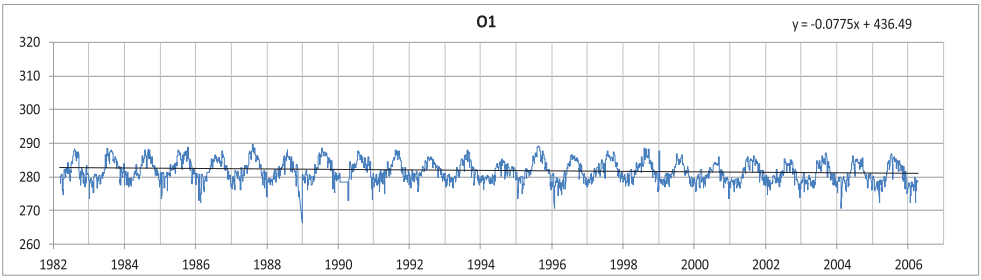

Figure 5: Temperature time series at ocean location O1, west of France.
Trend: -0.78 K/decade

Seven locations were selected because of their representative or anomalous behavior. These locations are shown superimposed on figure 2d. For these seven locations, 10 day filtered average temperature data were extracted and are plotted in figures 5 to 11. We have used the 10 day filtered data because they give a good impression of the yearly temperature cycle, which for the ocean locations (figure 5,6) is 5-10 K and much smaller than for the land locations (figure 7-11) where the amplitude is 15-30 K.

8. OBSERVATIONS

In general, the Atlantic Ocean, Africa and Europe show a negative temperature trend, varying between zero and -2 K/decade. Remarkable, is a large area in southern Africa, mainly Zimbabwe and Mozambique, where the temperature decrease is even larger and in the range of -2 to -3 K. Also note the temperature decrease of Lake Chad and Lake Nasser, probably due to an increase in their surface areas. There are also some spots that show a substantial temperature increase, in particular in SE Iraq (figure 3a) and NW Tanzania (figure 3b).

8.1. Ocean locations

The time series of the ocean locations O1 and O2 are presented in figure 5 and 6. The northern location (O1, ~45 N) shows a stronger yearly temperature cycle than the more

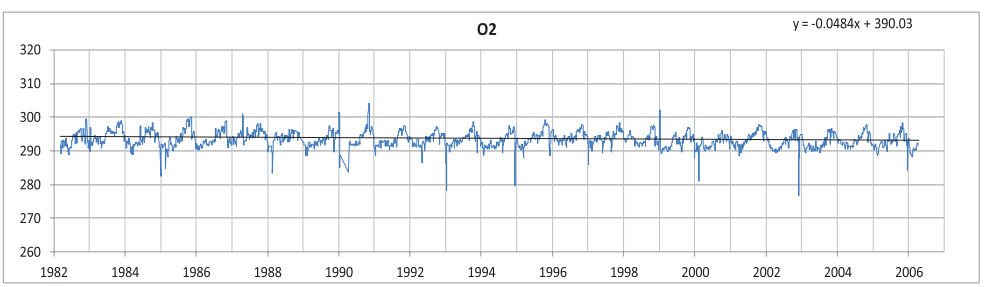

Figure 6: Temperature time series at ocean location O2, west of Senegal.
Trend: -0.48 K/decade

southern location (O2, ~15 N). This is related to the stronger variation in incoming solar radiation at the northern location. Figure 2d shows that the decrease in ocean surface temperature is smaller (-0.5 K/decade) at location O2 than elsewhere in the ocean. This location, west of Senegal and Mauritania, is known for upwelling of deeper ocean water. The temperature of the upwelling water is independent of energy balance at the ocean surface. When mixing with surface water this may weaken surface energy balance changes that cause the ocean surface temperature decrease.

8.2. Land locations

Figure 1c shows that in large parts of western and central Europe there is a significant surface temperature decrease, in the order of -1 to -2 K/decade. In the Po river basin, N France, the Benelux and the UK this decrease is less, but nowhere is an increase in average temperature found.

Figure 7 shows the temperature series as measured in France at location L1. The yearly amplitude is quite large: some 20-25 K. The temperature cycle at location L2 in Mauritania (figure 8) is only 15 K in amplitude, but the yearly average is some 20 K higher than in France. The trend at this location, and also in some other parts of Mauritania (figure 2d) is slightly negative (-0.5 K/decade).

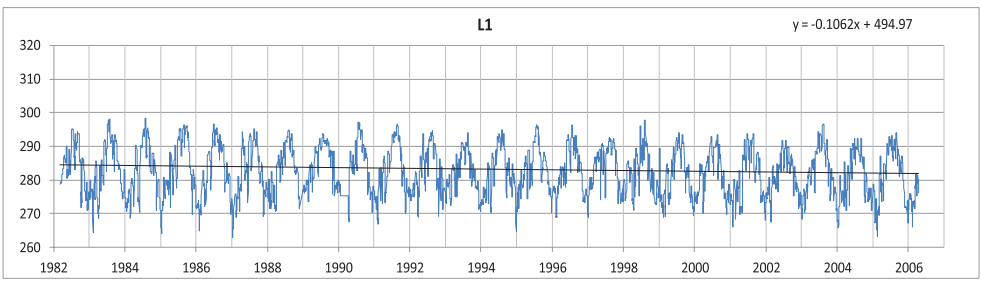

Figure 7: Temperature time series at land location L1, central France.
Trend: -1.1 K/decade

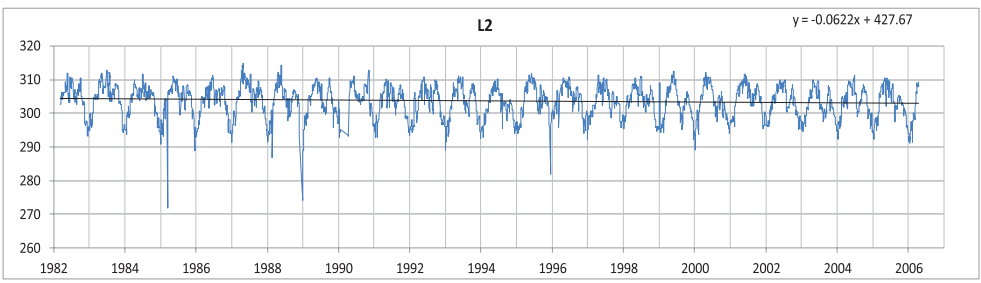

Figure 8: Temperature time series at land location L2, SE Mauritania.
Trend: -0.62 K/decade

The temperature decrease in Zimbabwe and Central Mozambique is very large, as much as -2 to -3 K/decade. This part of southern Africa is influenced by tropical cyclones from the Indian Ocean. The observed decrease may be due to the fact that there is a multi-yearly cycle in this phenomenon and the period 1986-1995 corresponds to one of minimum rainfall. After 1995, rainfall has increased again and this is the most likely cause of the observed strong decrease in temperature, which may be understood in terms of: (a) increased cloudiness and consequently a reduction in global radiation, and (b) increased soil water availability and increased evapotranspiration.

8.3 Anomalous spots

There are two small areas on the hemisphere where the temperature has increased significantly. The most extreme case is location L4 in SE Iraq, where a large average temperature increase is observed of 4.5 K/decade. A detail map of this area is shown in figure 3a. The corresponding temperature time series for this location is presented in figure 10. From the graph, it is clear that the temperature increase occurred in a short period from 1992 to 1995. The area is identified as marshes situated at the confluence of the Euphrates and Tigris. Under the regime of Saddam Hussein these marshes were drained to expel the Shiitic population from this area.

In Tanzania there is a small area in the northwest of the country (L5), where the temperature has increased by 1.1 K/decade (figure 3b). From the time series, shown in figure 11, it is concluded that this increase has been gradual. This location is in a mining area where activities have been expanding during the past decades. This will have led to an increase of open pits and tailings and consequently the disappearance of vegetation and a decrease of near surface water holding capacity, causing a decrease in evapotranspiration and consequently an increase of surface temperature.

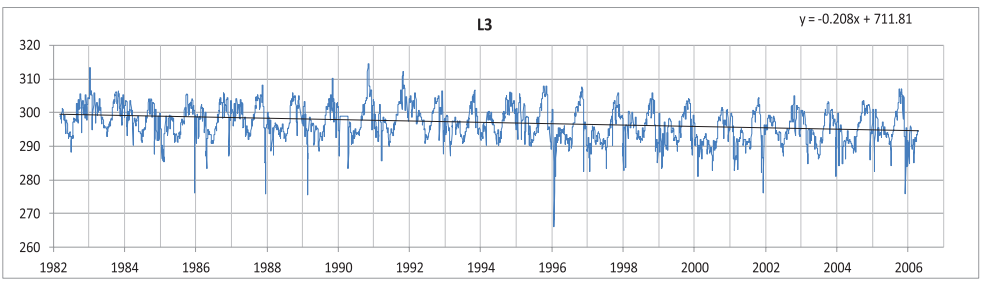

Figure 9: Temperature time series at land location L3 in southern Zimbabwe. Temperature trend: -2.1 K/decade. Most of the strong temperature decrease seems to have taken place during the period 1996-2001. This region in southern Africa periodically receives copious rainfall from Indian Ocean tropical cyclones. The period 1986-1995 was a period of low rainfall. Rainfall has increased thereafter, leading to increased cloudiness, decreased radiation and increasing evapotranspiration and consequently a temperature decrease.

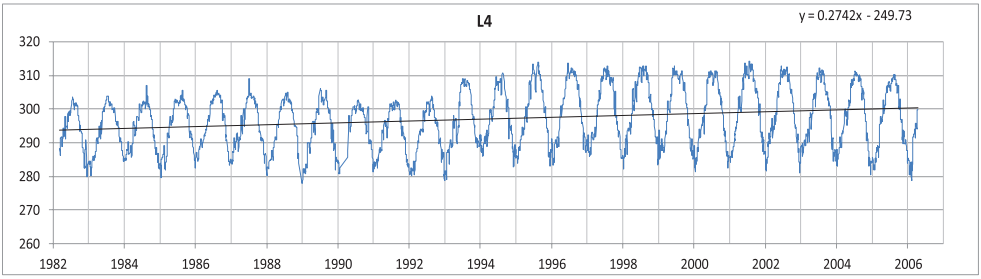

Figure 10: Temperature time series for land location L4 in SE Iraq. An exceptional location which shows a strong temperature increase of some 5K in the period of 20 year. This increase took mainly place in the period 1993-1995 and reflects the draining of the marshes at the confluence of the Ephrata and Tigris under the regime of Sadam Hussein.

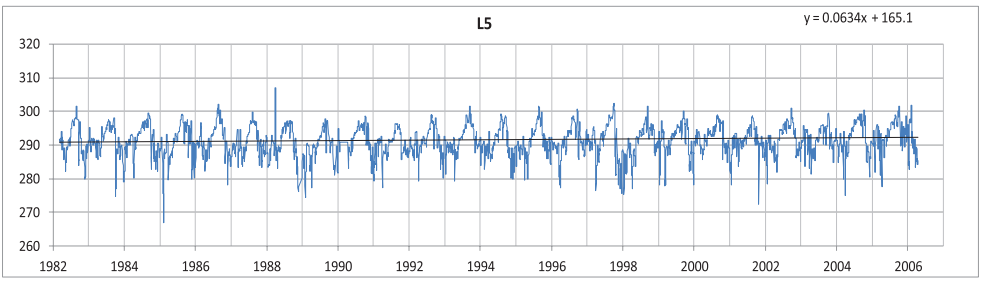

Figure 11: Temperature time series for land location L5 in NW Tanzania, south of Lake Victoria. There is a temperature increase of 1.3 K in 20 year. This location is in a strongly developing mining area. Decrease in vegetation cover and reduced evapotranspiration may have caused this temperature increase.

9. VALIDATION

The significant planetary temperature increase that has occurred in SE Iraq due to the draining of marshes, offers an opportunity to compare and validate the Meteosat observations. Figure 10 shows that the planetary temperature increase took place in three years, from 1992 to 1995. This temperature increase can only be related to the transition from wet to dry conditions, in other words should fall within the range of temperature change caused by a transition from potential to no evapotranspiration. This temperature change can be evaluated by means of surface energy balance calculations.

9.1 Determination of the observed, actual surface temperature change

But first, we have to convert the observed planetary temperature change into an actual earth surface temperature change. To this end we use the following relation

$$T_0 = T_0' + [(1-a*csi)/(a*csi)](T_0'-T_a) \quad (4)$$

Where T_0 is the surface temperature and T_0' the planetary temperature. The effect of the atmosphere is that the temperature difference across the boundary layer (T_0-T_a) is reduced to (T_0'-T_a). The reduction factor is defined as a= (T_0'-T_a)/ (T_0-T_a) for zero i.e. vertical viewing angle and is on average 0.65. The cosine of the viewing angle (csi) corrects for additional compression proportional to the path length. For the case of Basra, the viewing angle is some 45 degree and csi=0.71. The above expression then converts to:

$$T_0 = T_0' + 1.18\ (T_0'-T_a) \tag{5}$$

Assuming the temperature at the top of the boundary layer (T_a) to be constant we find for the change in actual surface temperature due to the transition from wet to dry:

$$\partial T_0 = 2.28 * \partial T_0' = 2.28*4.5 = 10.3\ K \tag{6}$$

9.2 Calculation of the theoretical surface temperature change

We will now calculate the theoretical change in surface temperature when going from wet to dry conditions. These calculations are based on the surface energy balance which may read:

$$I_{nc} = (1-A)I_g - \varepsilon_0(1-\varepsilon_a)\sigma T_a^4 = H_s + H_r + LE = (\alpha_s + \alpha_r + \alpha_l)(T_0-T_a) \tag{7}$$

The previous equation expresses that the climatic net radiation (I_{nc}) at the earth surface (first two terms) is equal to the sum of the sensible heat flux (H_s), radiative heat flux (H_r) and latent heat flux (LE) from the ground surface to the top of the atmospheric boundary layer. The forementioned heat fluxes are expressed in terms of the difference between the surface temperature (T_0) and the temperature at the top of the boundary layer (T_a). For the conditions in the marshes near Basra the heat exchange coefficients are estimated as follows:

$$\begin{aligned} \alpha_s &= C*v = 2*3 && = 6\ W/m^2K \\ \alpha_r &= 4\varepsilon_0\,\sigma T^3 && = 5\ W/m^2K \\ \alpha_l &= (L/c)(\partial s/\partial T)*\alpha_s && = 14\ W/m^2K \end{aligned} \tag{8}$$

C is the drag coefficient and v the windspeed. L is the heat of evaporation, c the volumetric heat capacity of air and s the specific air humidity. The short wave radiation component in (7) may be estimated with:

$$(1-A)*t*S/4 = (1-0.1)*0.85*1400/4 = 270\ W/m^2 \tag{9}$$

A is the surface albedo, t the atmospheric transmissivity and S the solar constant. The net long wave radiation is estimated with:

$$\varepsilon_0(1-\varepsilon_a)\sigma T_a^4 = 0.9*(1-0.8)*5.67E^{-8}*298^4 = 80\ W/m^2 \tag{10}$$

Here ε_0 is the surface emissivity and ε_a the effective downward atmospheric emissivity. Thus the climatic net radiation I_{nc} is estimated at 270-80 = 190 W/m^2. We may now express the energy balance for the wet and the dry situation in terms of the surface temperature difference across the boundary layer (T_0-T_a). For the wet and the dry situation, respectively, we have:

$$190 = (\alpha_s + \alpha_r + \alpha_l)(T_0 - T_a) = 25*(T_{0w} - T_a) \quad \text{(wet)}$$
$$190 = (\alpha_s + \alpha_r)(T_0 - T_a) = 11*(T_{0d} - T_a) \quad \text{(dry)}$$

or

$$T_{0w} - T_a = 190/25 = 7.6 \text{ K}$$
$$T_{0d} - T_a = 190/11 = 17.3 \text{ K} \qquad (11)$$

Assuming the top of the boundary layer temperature (at 1-2 km height) not to change, we obtain the following theoretical increase in earth surface temperature on the transition from wet to dry:

$$T_{0d} - T_{0w} = 17.3\text{-}7.6 = 9.7 \text{ K} \qquad (12)$$

The observed earth surface temperature change on the transition from wet to dry (10.3 K) is about equal to the theoretically derived temperature change (9.7 K). This is an argument in favor of the validity of the Meteosat temperature observations. A hypothetical trend correction, that would give some warming, would have to be 1.0-1.5 K upward. Such an upward correction would increase the observed planetary temperature anomaly near Basra from 4.5 to 5.5 or 6.0 K. The corresponding surface temperature increase would then become 12.5-13.7 K, which is much too high compared to the theoretical temperature increase of 9.7 K. Therefore an upward trend correction is to be rejected.

10. CONCLUSION

The amazing finding of the present study is that we do not observe global warming in the period 1982-2006, but significant cooling. What could be the cause?

The satellite data are from a reliable origin supported by the European meteorological community. Their accurate calibration has received due attention and efforts from Eumetsat. Our processing of these data has been simple and straight forward, involving only noon and midnight image composition, averaging and a filter to eliminate cloud effects. We have created similar planetary temperature change images for the unfiltered, 10, 20 and 30 day filtered data, clearly showing convergence towards the longer filters, indicating that cloud influences were effectively removed. Moreover, we do observe significant temperature increase at some locations which are due to human interventions, and which are quantitatively in line with the theoretically expected effects of these interventions. Therefore we believe the observed planetary temperature decrease for most of the hemisphere to be real.

The cloud filtered temperature change patterns, in figure 2c, indicate that the largest decrease occurs in the more cloudy regions of the hemisphere: the tropics and the temperate zones, while in the desert belt the temperature decrease is much smaller.

This suggests that cloudiness changes could be the mechanism behind the observed global cooling since 1982: an increase in cloudiness would decrease global radiation and increase rainfall and evapotranspiration. Both effects tend to decrease the surface temperature.

REFERENCES

1. Rosema A (1993) *Using Meteosat for Operational Evapotranspiration and Biomass Monitoring in the Sahel Region*, Remote Sens. Envir. 45:1-25.
2. Rosema A, DeWeirdt M, Foppes S (2010a) *Monitoring and Early Warning*, in: Applied Agrometeorology, K Stigter (ed.) Springer, Hiedelberg.
3. Rosema A, De Weirdt M, Foppes S, Wilczok (2010b) *FESA Micro-Insurance: Methodology, validation, contract design*, Report Millennium Project 38, DG for International Cooperation, Ministry of Foreign Affairs, the Netherlands
4. Christy JR, Norris WB, Spencer RW, Hnilo JJ (2007) *Tropospheric temperature change since 1979 from tropical radiosonde and satellite measurements*, Journal of Geophysical Research 112
5. Spencer RW and Christy JR (1990) *Precise monitoring of global temperature trends from satellites*, Science, 247, 1558-1565
6. Mears CA, Wentz FJ (2005) *The effect of diurnal correction on satellite derived lower tropospheric temperature*. Science, 309, 1548-1551
7. Trenberth KE, Jones PD, Ambenje P, Bojariu R, Easterling D, Klein Tank A, Parker D, Rahimzadeh F, Renwick JA, Rusticucci M, Zhai P (2007) *Observations: Surface and Atmospheric Climate change,* Climate change 2007: the Physical Science Basis. Contribution of Working Group 1 to the Fourth Assessment Report of the Inter-governmental Panel on Climate Change
8. http://www.eumetsat.int/Home/Main/DataProducts/Calibration/MFGCalibration/index.htm